Electrochimica Acta 367 (2021) 137474

Contents lists available at ScienceDirect

Electrochimica Acta

journal homepage: www.elsevier.com/locate/electacta

Synthesis of high-performance electrochromic material for facile fabrication of truly black electrochromic devices

Fang-Wei Li [a], Tzu-Chieh Yen [a], Guey-Sheng Liou [a,b,*]

[a] Institute of Polymer Science and Engineering National Taiwan University, No. 1, Sec. 4, Roosevelt Rd., Taipei 10617, Taiwan
[b] Advanced Research Center for Green Materials Science and Technology National Taiwan University, Taipei 10617, Taiwan

ARTICLE INFO

Article history:
Received 11 September 2020
Revised 5 November 2020
Accepted 11 November 2020
Available online 26 November 2020

Keywords:
Electrochromism
Triphenylamine
Dimethylamino
Polyamide
ZrO_2 Hybrid

ABSTRACT

A high-performance electrochromic polyamide, NPTB-PA, derived from *N,N′*-bis(4-(dimethylamino)phenyl)-*N,N′*-di(4-aminophenyl)-4,4′-biphenyldiamine (NPTB-diamine) demonstrates important characteristics of multi-oxidation stages and lower oxidation potentials due to the stronger electron-donating ability of dimethylamino groups. Besides, functional hydroxyl groups on the polymer backbone could be conducted via in-situ sol-gel reaction to form covalent bonds between polymer back-bones and precursor of zirconium dioxide (ZrO_2), and the resulted hybrid films could shorten the switching response time and reduce oxidation redox potentials through electron donor-acceptor system during the electrochemical processes. In addition, anodic electrochromic polyamide NPTB-PA and cathodic heptyl viologen (HV) were introduced into the electrochromic device (ECD) to construct ambipolar system, and the obtained ECD exhibited the panchromatic absorption from transparent to truly black during oxidation (NPTB-PA)/reduction (HV) process with extremely high contrast of transmittance change (ΔT) of 80% over the whole visible-light region. This excellent combination is unique and facile for fabricating novel panchromatic advanced ECD shutter with only two redox-active materials.

1. Introduction

With the development of science and technology, various optoelectronic materials have grabbed lots of attentions. Among them, one of the most essential optoelectronic materials is the electrochromic materials (ECMs), which can exhibit different colours during their redox processes [1–3], and can be used for different kinds of applications, such as tunable anti-glare car rearview mirrors, low power consumption items, smart windows and so forth [4–6]. Therefore, various representative ECMs have been developed and studied for decades, which could be classified into four main categories: transition-metal oxides (e.g., tungsten trioxide (WO_3) [7–9]), metal coordination complexes (e.g., Prussian blue (PB) [10–11]), conjugated conducting polymers (e.g., Poly(thiophene)s (PTs) [12–13]), and organic molecules (e.g., viologens [14–15]). For the sake of investigating the potential applications of ECMs to meet the demands of consumers, many ECMs with various molecular structures were designed and utilized to fabricate the electrochromic devices (ECDs), and could be divided into two operational modes: transmission or reflection according to the type of color modulation [16].

Since 2005, our research group has published a series of triphenylamine-based (TPA-based) polymers that possess several characteristic features, such as high contrast ratio of transmittance between bleaching and coloring states, excellent thermal stability, outstanding coloration efficiency, and multiple color changes within the same one molecular chain [17–19]. Moreover, these polymers with TPA moieties are usually soluble in polar aprotic amide solvents because of the bulky and non-coplanar propeller-like shape, resulting in beneficial processing property for applications. Furthermore, TPA moiety with dimethylamino group at the para position of phenyl reveals stronger electron-donating ability than methoxy group and also demonstrates the capability to prevent coupling reaction at the same time, yielding not only lower oxidation potentials but multiple oxidation states [20,21]. In order to enhance the EC properties, we have attempted to design various polymers with hydroxyl groups (-OH) or carboxylic groups (-COOH) which could serve as active sites to conduct in-situ sol-gel reaction with precursors of metal oxides (for e.g., TiO_2, ZrO_2). The obtained donor-acceptor hybrid system could facilitate the charge transfer interactions during redox process. This facile but judicious approach could effectively reduce redox driving potentials, enhance

* Corresponding author at: Institute of Polymer Science and Engineering and Advanced Research Center for Green Materials Science and Technology, National Taiwan University, Taipei 10617, Taiwan.
E-mail address: gsliou@ntu.edu.tw (G.-S. Liou).

https://doi.org/10.1016/j.electacta.2020.137474
0013-4686/

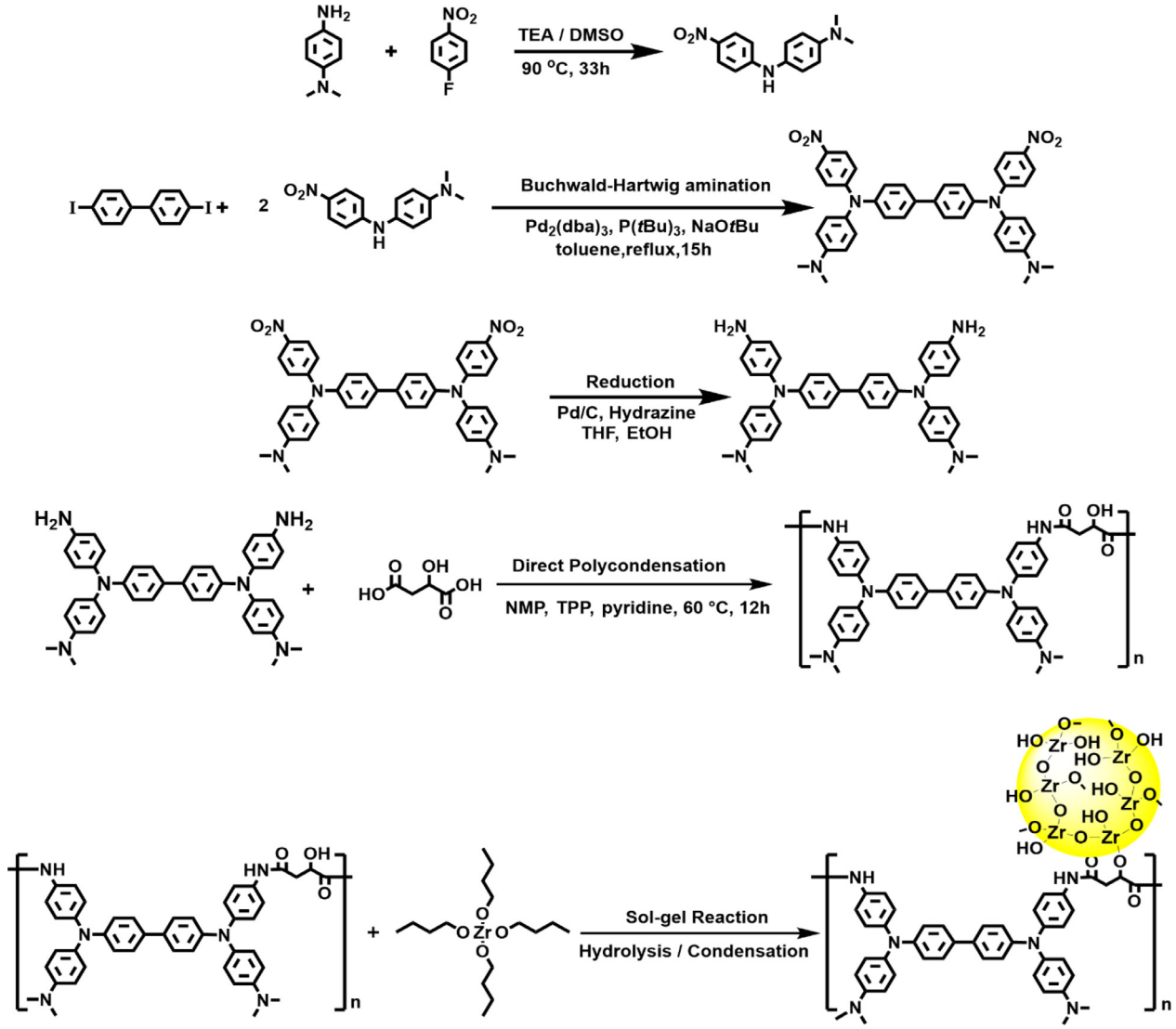

Scheme 1. Synthesis routes of diamine monomer, polyamide and hybrids.

switching response capability and adhesion to the ITO-coated glass substrate [22–24].

Recently, "transmissive-to-black" ECDs have been successfully designed and fabricated [25,26], while with the drawbacks of higher driving voltage and longer switching response time. For producing the panchromatic ECDs, it is critical and essential to Fig. out the complementary absorption characteristics from various ECMs for obtaining the absorption of full-wavelength band over the visible light region and turn to "black" switching state from neutral transparent bleaching state during redox processes. Besides, some crucial factors also need to be taken into consideration for practical applications, including optical contrast ratio between bleaching and coloring states, electrochemical stability, and response capability.

In this study, a novel TPA-based derivative, *N,N′*-bis(4-(dimethylamino)phenyl)-*N,N′*-di(4-aminophenyl)−4,4′-biphenyldiamine (NTPB-diamine), was successfully synthesized and used to prepare polyamide with malic acid. Furthermore, the NTPB-PA/ZrO_2 hybrid films with nano-domain dispersed structures could be obtained through in-situ sol-gel hybridization approach. Compared to simple NTPB-PA, the polymer structure obtained through sol-gel reaction shows stronger electron-withdrawing ability, which contains ZrO_2 that could store the electrons released from the electron-donating TPA moieties in the oxidation process. Precisely because of it, while in the ~~reverse~~ process of reduction, they would transfer the electrons back to the TPAs rapidly. Therefore, the donor-acceptor hybrid materials could effectively enhance the EC performance in terms of response capability. In addition, NTPB-PA could be readily fabricated to the gel-type ECD with heptyl viologen (HV) [27–30] for charge balance based on ambipolar complementary system and the obtained devices demonstrate excellent absorption band-merging design concept. This judicious combination is unique and facile for obtaining novel panchromatic advanced ECD shutter with only two ECMs.

2. Results and discussion

2.1. Monomer and polymer synthesis

The new diamine with *N,N,N′,N′*-tetraphenylbenzidine (TPB) unit, *N,N′*-bis(4-(dimethylamino)phenyl)-*N,N′*-di(4-aminophenyl)−4,4′-biphenyldiamine (NTPB-diamine), was acquired through heterogeneous Pd/C-catalyzed transfer hydrogenation of the nitro compound, *N,N′*-bis(4-(dimethylamino)phenyl)-*N,N′*-bis(4-nitroyphenyl)−4,4′-biphenyldiamine (NTPB-dinitro), resulting from Buchwald-Hartwig amination of *N,N*-dimethyl-

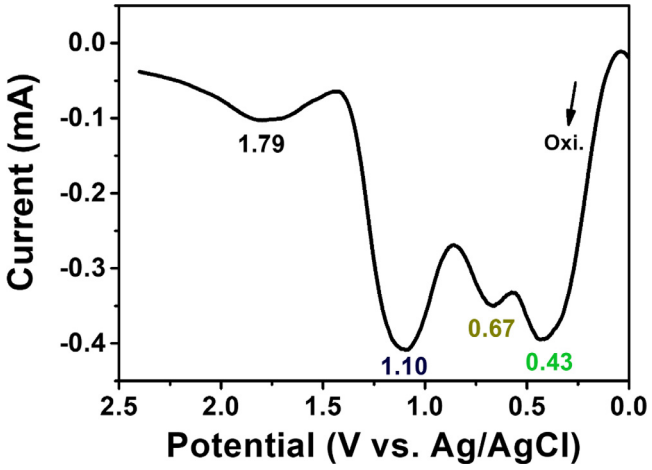

Fig. 1. Differential pulse voltammetric diagram of NTPB-PA film on the ITO-coated glass substrate in 0.1 M $TBABF_4$/MeCN at the scan rate of 2 mV/s; pulse amplitude: 50 mV; pulse width: 25 ms; pulse period: 0.2 s.

N'-(4-nitro-phenyl)-p-phenylenediamine (NDPA-nitro) [31] and 4,4′-diiodobiphenyl, and the complete procedures are illustrated in Scheme 1. FT-IR and NMR spectra were used to identify structures of the new intermediate NTPB-dinitro and targeted NTPB-diamine. (Fig. S1-S10). All characteristic peaks confirmed the proposed molecular structures. The nitro groups of NTPB-dinitro appeared at around 1590 and 1310 cm^{-1} (Fig. S10b) which represent NO_2 asymmetric and symmetric stretching. After the reduction of NTPB-dinitro, the characteristic peaks of primary NH_2 group of NTPB-diamine appeared at round 3400 (N–H stretching) and 1605 (N–H scissoring) cm^{-1} to replace NO_2 group, indicating that the reaction proceeded successfully.

According to phosphorylation technique [32–34], polyamide (NTPB-PA) was synthesized from the diamine monomer (NTPB-diamine) and dicarboxylic acid (malic acid) in NMP by conventional direct polycondensation by using TPP and pyridine as condensing agents as shown in Scheme 1 and the Supplementary Information. The molecular weights and solubility property of the obtained polymer are summarized in Table S1 and Table S2. The thermal properties of NTPB-PA were investigated by TGA (Fig. S11) and DSC (Fig. S12), and these results are listed in Table S3. NTPB-PA exhibited high thermal stability without significant weight loss up to 375 °C under nitrogen or air atmosphere even the incorporation of aliphatic moieties, and glass-transition temperatures (Tg) of NTPB-PA was 206 °C caused by the rigidity of NTPB structure. Further, hydroxyl-containing NTPB-PA provides reactive sites to conduct in-situ sol-gel reaction with different weight percentages of ZrO_2 precursor. And NTPB-PAZrX was used to denote EC hybrid films with different contents of ZrO_2, where X is the wt% value of ZrO_2. The preparation of the hybrid films was described in Scheme 1 and the Supplementary Information.

2.2. Optical and electrochemical properties of the polyamide NTPB-PA

2.2.1. Electrochemical properties

The electrochemical properties of the redox-active polyamide NTPB-PA were investigated by cyclic voltammetry (CV) and differential pulse voltammetry (DPV) conducted by casting film on the ITO-coated glass substrate (30 mm × 7 mm) as a working electrode, platinum wire as an auxiliary electrode, and Ag/AgCl in 0.3 M KCl as a reference electrode in 0.1 M $TBABF_4$/MeCN. The electron-donating dimethylamine substituents at the para-position of phenyl groups in **NTPB-PA** could effectively prevent the coupling reaction by affording stable cationic radicals and lowering the oxidation potentials [35,36]. The representative DPV diagram of **NTPB-PA** depicted in **Fig. 1** reveals four obvious oxidation peaks. The first and the second oxidation states are more useful for practical application owing to their lower oxidation potentials and higher electrochemical stability. Hence, the subsequent hybrid effects would be focused on the first and the second oxidation peaks. All the CV diagrams and their partial magnifications are depicted in **Fig. 2**, and the related values are also summarized in Table 1. The first and the second oxidation potentials of **NTPB-PAZr0** (0.34 and 0.78 V) were higher than those of **NTPB-PAZr5** (0.33 and 0.73 V) and **NTPB-PAZr10** (0.24 and 0.70 V). Besides, the value of redox potential difference between the oxidation and reduction peaks, ΔE, became smaller in the case of higher weight percentage of ZrO_2. Smaller value of ΔE represents faster electron transfer rate and lower driving force of redox process [37]. These results indicate that ZrO_2 could build up a remarkable donor-acceptor system to facilitate electron transfer between TPA and ZrO_2 units, resulting in higher EC performance. Furthermore, coloration efficiency of the hybrid polymer films could also increase with the content of metal oxide as shown in Table S4. Thus, we speculate the metal oxide could not only serve as donor-acceptor system but may enhance the ability of capacitance that would produce higher coloration efficiency.

2.2.2. Spectroelectrochemical properties

Spectroelectrochemical measurements were conducted for evaluating the optical behavior of the EC films by optical spectroscopy. The cuvette was placed in the path of light beam in a UV–vis-NIR spectrophotometer, which allows us to acquire absorption spectra under applied potential. The typical spectroelectrochemical data and the corresponding color appearance are depicted in Fig. 3. The polyamide film exhibited a transparent pale-yellowish color at neutral state (0 V) without any applied voltage. Upon oxidation from 0 to 0.6 V, the characteristic absorption band generated from 600 to 1000 nm associated with strong green color could be observed (Fig. 3a).

The first oxidation reversibility was 98.5% based on the absorbance at 315 nm. As the applied potential continued to increase to the second oxidation state, the new absorbance peaks at 478, 756 nm and a broad intervalence charge-transfer (IV-CT) characteristic band around at 1380 nm appeared when applying potential increased from 0.7 to 0.9 V (Fig. 3b) [38,39], and the reversibility was 95.6% for the second oxidation state. When the applied potential was raised to the third oxidation state from 1.0 to 1.2 V, the value of absorbance over the whole visible spectrum is almost larger than 1.5 times, indicating this oxidized coloring state is a truly black form (Fig. 3c) with a reversibility of 94.2%. In addition, the absorption spectrum of HV shown in Fig. S13 reveals that it is colorless at the original form (0 V) and exhibits characteristic peak at 400 nm and broad band around 600 nm during their reduction process (HV^{2+} to HV^{1+}). Therefore, with the introduction of HV into the system, the absorption characteristics for anodic ECM of **NTPB-PA** (2nd oxidation state) and cathodic ECM of HV could be merged complementarily to form a truly black ECD based on using these two ECMs.

2.2.3. Electrochromic switching properties

EC switching response was used to record the change of optical transmittance as a function of time between coloring and bleaching state at the specified absorption wavelength. The switching time was determined as the time reaching 90% of the full switch in transmittance. From the spectroelectrochemical data in Fig. 3, the characteristic peaks at 478 and 756 nm were chosen to display the response capability at the second oxidation state of all the EC films. According to the Fig. 2, the value from 0.9 and −0.2 V were set as applied potential for completing oxidation and reduction of these

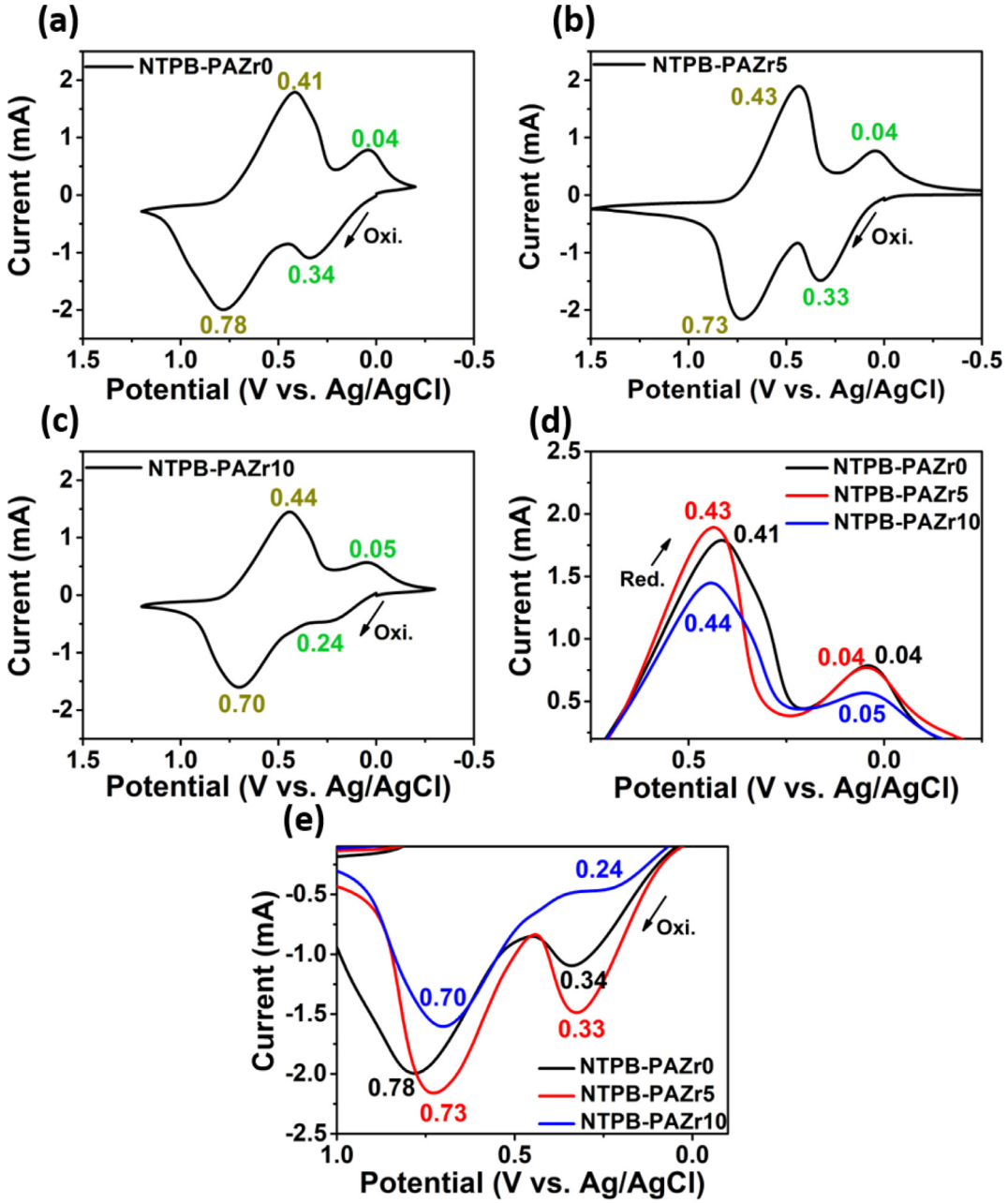

Fig. 2. Cyclic voltammetry diagrams of (a) **NTPB-PAZr0** (720 ± 20 nm), (b) **NTPB-PAZr5** (930 ± 15 nm), (c) **NTPB-PAZr10** (1020 ± 25 nm), the partial magnification of (d) oxidation peaks of hybrid films and (e) reduction peaks of hybrid films on ITO-coated glass substrates (deposited area: 3.0 cm × 0.7 cm) in 0.1 M $TBABF_4$/MeCN at the scan rate of 50 mV/s.

Table 1
Redox potentials[a] and potential differences of the films.

Films	1st Oxidation state			2nd Oxidation state		
	$E_{oxi.}$[b] (V)	$E_{red.}$[c] (V)	ΔE[d] (V)	$E_{oxi.}$[b] (V)	$E_{red.}$[c] (V)	ΔE[d] (V)
NTPB-PAZr0	0.34	0.04	0.30	0.78	0.41	0.37
NTPB-PAZr5	0.33	0.04	0.29	0.73	0.43	0.30
NTPB-PAZr10	0.24	0.05	0.19	0.70	0.44	0.26

[a] Measured relative to Ag/AgCl in 0.1 M $TBABF_4$/MeCN.
[b] Oxidation potential at the peak.
[c] Reduction potential at the peak.
[d] Potential difference between oxidation and reduction peaks, $|E_{oxi.} - E_{red}|$.

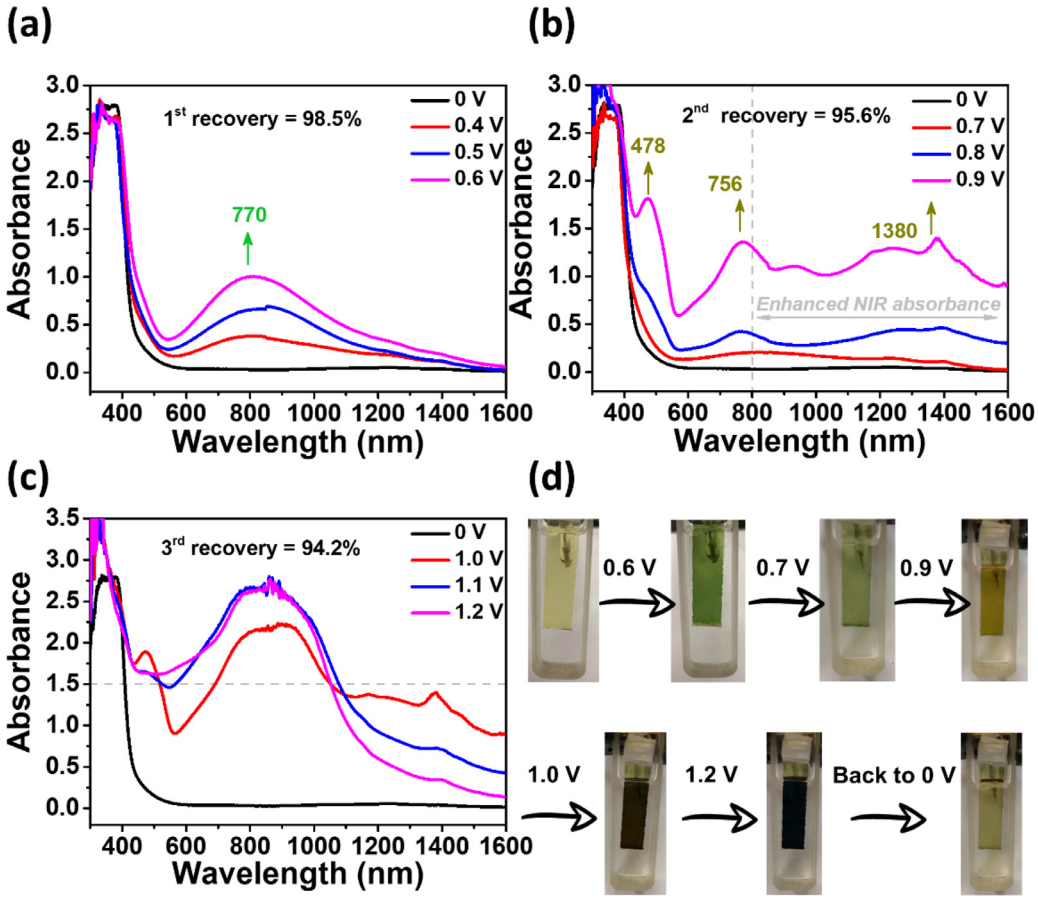

Fig. 3. Absorbance spectra for (a) first oxidation state (b) second oxidation state and (c) third oxidation state of NTPB-PA film on the ITO-coated glass substrates in 0.1 M $TBABF_4/CH_3CN$ at the applied potential from (a) 0–0.6 V, (b) 0.7–0.9 V, (c) 1.0–1.2 V (V vs. Ag/AgCl) and (d) the corresponding color appearance.

Table 2
Switching response time of the films.

Films	478 nm		756 nm	
	t_c [a] [s]	t_b [b] [s]	t_c [a] [s]	t_b [b] [s]
NTPB-PAZr0	12.5	15.0	18.0	18.0
NTPB-PAZr5	11.5	11.5	17.5	9.5
NTPB-PAZr10	9.5	9.0	15.5	5.5

[a] Timescale at oxidation state reaching 90% of the full switch in transmittance.
[b] Timescale at reduction state reaching 90% of the full switch in transmittance.

EC films during coloring and bleaching process, respectively. The final results are illustrated in Figs. 4 and 5, and also summarized in Table 2. The pristine polyamide film, **NTPB-PAZr0** (Figs. 3a and 4a), needed 12.5 s for coloring and 15 s for bleaching at the absorption wavelength of 478 nm, and 18 s for coloring and 18 s for bleaching at 756 nm, respectively. Then, with the amount of ZrO_2 increasing, such as **NTPB-PAZr5** (Figs. 3b and 4b) and **NTPB-PAZr10** (Figs. 3c and 4c) that could shorten the switching time by degrees. Consequently, the hybrid films demonstrate the effect on response time, especially for the bleaching time which confirms the influence of ZrO_2 acting as electron storage moiety. Finally, the coloring time and bleaching time of **NTPB-PAZr10** could be reduced to 9.5 s and 9 s at 478 nm and 15.5 s and 5.5 s at 756 nm, respectively, indicating that this facile approach should be feasible and with high potential to be utilized in display applications especially for the case of thicker EC film.

2.2.4. Electrochemical stability tests

There are several methods to display the electrochemical stability of ECMs. Herein, the stability of **NTPB-PA** was determined by measuring the optical change as a function of the number of switching cycles by chronoamperometric and absorption measurements. The EC stability of the first and second oxidation states was confirmed for the further applications. The amount of optical density (δOD) could be obtained by taking the form of logarithm between $T_{colored}$ and $T_{bleached}$ from Fig. 6 to Fig. S14. The amount of Q was calculated by integration of the current density and time. The EC coloration efficiency (CE $= \eta = \delta$ OD/Q) was 163.7 cm^2/C for the case of 770 nm at the first oxidation state. And the decay of transmittance (ΔT decay) after 500 cycles was only less than 5%. As the applied potential increased to the second oxidation state, the CE was up to 179.9 cm^2/C at 756 nm, and all the results are summarized in Table 3 and Table S5.

2.2.5. Electrochemical impedance spectroscopy (EIS)

EIS is response of the system as a function of the perturbation frequency revealing internal dynamics. The function for impedance ($Z(\omega)$) is composed of a real part on the X-axis and an imaginary part on the Y-axis, which constructs the Nyquist plot (as shown in Fig. 7). Herein, the plot was fitted by Randles circuit, where the solution resistance (R_Ω) is in series with a parallel combination of a double-layer capacitance (C_{dl}) and an impedance of charge transfer resistance (R_{ct}) and Warburg element (Z_W). At the high frequency intercept, the real axis value gives the solution resistance (R_Ω). The low frequency intercept of the real axis provides a summation of the charge transfer resistance and the solution resistance. Therefore, the semicircle diameter will equal the charge transfer resis-

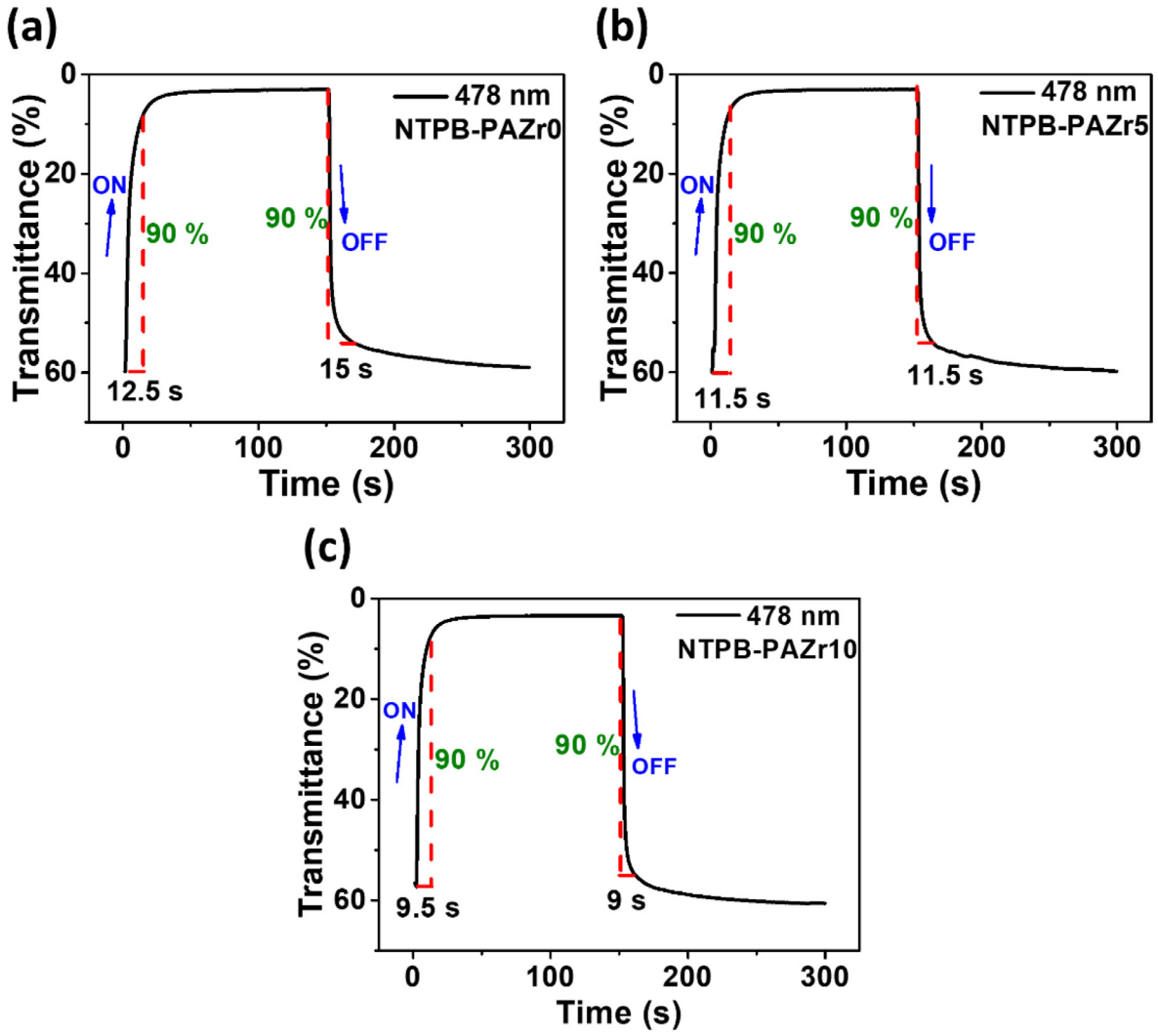

Fig. 4. Switching response time of (a) **NTPB-PAZr0** (720 ± 20 nm), (b) **NTPB-PAZr5** (930 ± 15 nm) (c) **NTPB-PAZr10** (1020 ± 25 nm) films on ITO-coated glass substrates (deposited area: 3.0 cm × 0.7 cm) in 0.1 M $TBABF_4$/MeCN between 0.9 V (ON) and −0.2 V (OFF) at the characteristic absorption peak of 478 nm.

Table 3
Optical and electrochemical data of **NTPB-PA** at the first oxidation potential.

Cycling times[a]	ΔT (%)[b]	δOD[c]	ΔT decay (%)[d]
1	36.0	0.221	0
100	35.8	0.216	0.6
200	35.8	0.216	0.6
300	35.4	0.216	1.7
400	34.7	0.214	3.6
500	34.4	0.210	4.4

[a] Switching between 0.48 and −0.2 V.
[b] Transmittance change at 770 nm.
[c] Optical density (δOD) = log [$T_{bleached}/T_{colored}$], where $T_{bleached}$ and $T_{colored}$ are the maximum transmittance in the oxidized and neutral states, respectively.
[d] Decay of transmittance after cyclic scans = (ΔT_0 - ΔT)/ΔT_0 × 100%.

tance (R_{ct}). To study the diffusion rate of the charge during the redox process, R_{ct} is an important parameter and the calculated values under different applied potentials (0.48 and 0.9 V for coloring state at different oxidation states and 0 V for bleaching state) are summarized in Table 4. The tendency is similar no matter which potential was applied. For example, the pristine polyamide film of **NTPB-PAZr0** exhibited the highest values of R_{ct} (49.6 Ω at 0.9 V, 56.3 Ω at 0.48 V, and 92.1 Ω at 0 V) among these three EC films, implying the slowest electron transfer rate. While, along with the introduction of ZrO_2, the value of R_{ct} reduced with increasing the amount of ZrO_2 up to 10 wt% that is an obvious evidence toward the effects of hybrid system, indicating higher hybrid content could bring forth the smaller value of R_{ct}, higher electron transfer rate, and thus shorter switching response time.

2.3. Optical and electrochemical properties of ECDs

2.3.1. Electrochemical properties

For further applications, the **NTPB-PA** film was chosen to fabricate ECDs. The preparation procedure of the ECDs is depicted in Fig. S15 and Fig. S16. Then, CV was used to investigate EC behavior of the obtained gel-type ECDs. The devices with 120 μm gap and 4 cm^2 active area were comprised of two ITO-coated glass substrates, one piece of ITO-coated glass substrate was covered by **NTPB-PA** film. Owing to the larger active area and gel-type electrolyte, the rate of ion diffusion would decrease, resulting in the higher driving voltage. With the help of HV, the potential for the first oxidation stage could be reduced from 1.86 to 1.27 V as shown in Fig. S17. This phenomenon could be attributed to the role of HV as charge trapping layer which facilitates charge balance during EC switching, indicating that HV^{2+} could accept electrons from oxida-

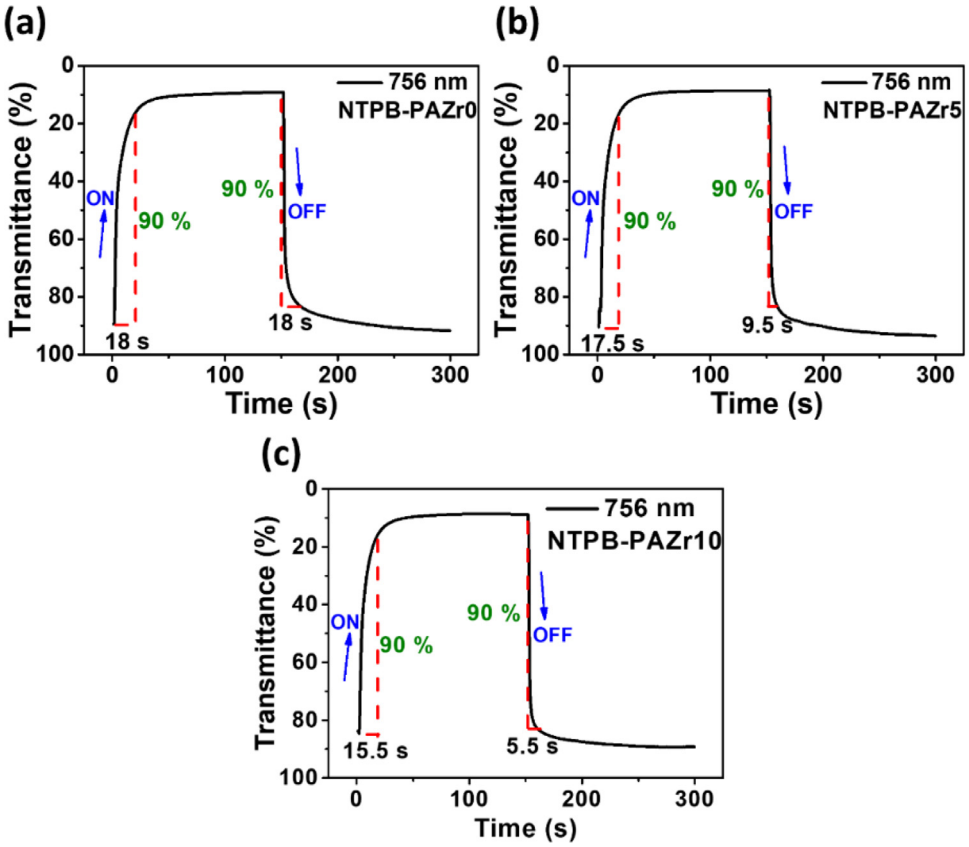

Fig. 5. Switching response time of (a) NTPB-PAZr0 (720 ± 20 nm), (b) NTPB-PAZr5 (930 ± 15 nm) (c) NTPB-PAZr10 (1020 ± 25 nm) films on ITO-coated glass substrates (deposited area: 3.0 cm × 0.7 cm) in 0.1 M $TBABF_4$/MeCN between 0.9 V (ON) and −0.2 V (OFF) at the characteristic absorption peak of 756 nm.

Table 4
Solution resistance (R_Ω) and charge transfer resistance (R_{ct}) from the Nyquist plot at different applied potentials.

Films	0 V (bleaching state)		0.48 V (coloring state)		0.90 V (coloring state)	
	R_Ω[a] (Ω)	R_{ct}[b] (Ω)	R_Ω[a] (Ω)	R_{ct}[b] (Ω)	R_Ω[a] (Ω)	R_{ct}[b] (Ω)
NTPB-PAZr0	4.08	92.1	4.29	56.3	3.91	49.6
NTPB-PAZr5	4.12	72.0	3.93	50.7	3.90	46.2
NTPB-PAZr10	4.03	57.5	3.97	38.9	4.11	33.7

[a] Obtained from interception of the Nyquist plots on the real axis.
[b] Obtained from the diameter of the semi-circle or the arc.

tion centers of **NTPB-PA**, and then HV^+ also could donate electrons back to the oxidized units during reduction (NTPB-PA)/oxidation (HV) process. From CV diagram, HV reveals the effect to compensate the drawbacks caused by gel-type electrolyte approach and demonstrates the positive influence on overall ECD system.

2.3.2. Spectroelectrochemical properties

Typical spectroelectrochemical data of the resulted ECDs are presented in Fig. 8 and Fig. S18. By incorporation of HV into the ECD, the characteristic absorption peak attributed to HV at around 600 mm appeared. In addition, the characteristic absorption peaks derived from both **NTPB-PA** and HV could be successively matched to achieve excellent complementary panchromatic color-merging effect.

UV–vis transmittance curves correlated to applied voltages of **NTPB-PA/HV** ECD are depicted in Fig. 9a. It is extremely remarkable that only two ECMs could absorb very complementarily and completely over the whole visible light region (400–800 nm) with the incredible low transmittance value less than 1% subsequent to the applied voltage at 1.7 V as illustrated in Figs. 8 and 9. As the photos shown in Fig. 9b, **NTPB-PA/HV** ECD manifested the genuine and authentic black EC behavior at the coloring state. Consequently, the results demonstrate that this study reveals a facile and judicious design for fabricating a truly panchromatic black display.

3. Conclusion

A high-performance polymer, **NTPB-PA** exhibited high thermal stability, good adhesion to ITO-substrate and multi-color EC behaviors at the different oxidation states. Besides, the reactive hydroxyl functional groups on polymer backbones could form covalent bonds with the precursor of ZrO_2 through *in-situ* sol-gel hybridization approach. The resulted hybrid film of **NTPB-PAZr10** revealed the enhancement of electrochemical characteristics, such as lower oxidation potentials (reducing from 0.34 to 0.24 V and from 0.78 to 0.70 V for the first and second oxidation potentials, respectively), faster switching response time (from 12.5 to 9.5 s and from 15 to 9 s for coloring time and bleaching time at 478 nm, and from 18 to 15.5 s and from 18 to 5.5 s for coloring time and bleaching time at 756 nm, respectively) and smaller charge transfer resistance, R_{ct} (from 56.3 to 38.9 Ω and from 49.6 to 33.7 Ω for the first and the second oxidation potentials, respectively). Con-

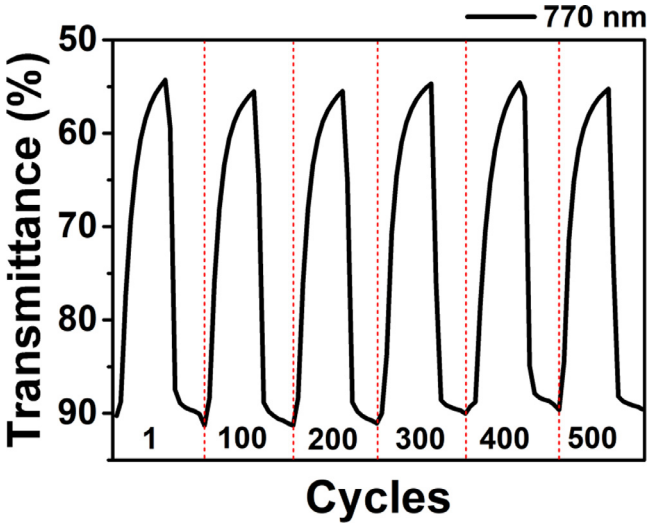

Fig. 6. EC repetitive switching response of NTPB-PA (200 ± 10 nm) on ITO-coated glass substrates (deposited area: 3.0 cm × 0.7 cm) between 0.48 V (ON) and −0.2 V (OFF) at the characteristic peak 770 nm in 0.1 M $TBABF_4$/MeCN with a cycle time of 30 s for 500 cycles.

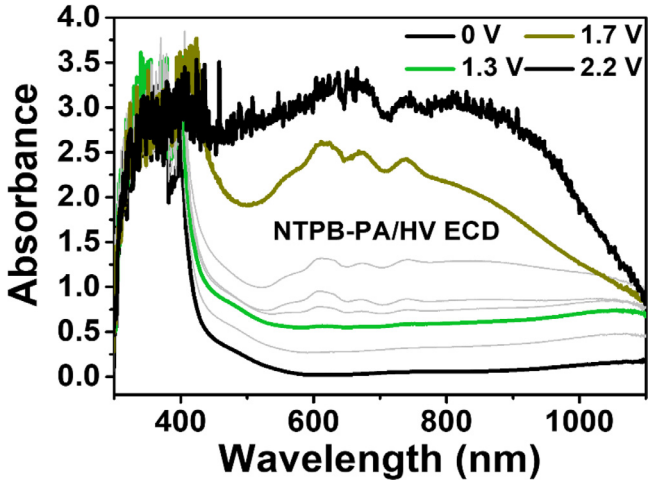

Fig. 8. Absorbance spectra of **NTPB-PA/HV** gel-type ECD (deposited area: 20 mm × 20 mm) in 0.1 M (5 μmole) $TBABF_4$/PC at different applied potential.

sequently, new polyamide **NPTB-PA** prepared in this study would be a high performance ECM with impressive potential as candidate for applications. In addition, HV could be introduced into the ECDs to construct a novel "transmissive-to-black" ECD based on the ambipolar system. The resulting ECD demonstrates high significant transmittance change (ΔT) of 80% in visible region, indicating the genuine and authentic black EC behavior at coloring state could be attained. Hence, the novel advanced ECD as truly panchromatic black display was successfully fabricated by using only two ECMs, **NTPB-PA** and HV.

4. Experimental section

Materials: Fluoro-4-nitrobenzene (99%, Acros), *N,N*-dimethy-*p*-phenylenediamine (97%, Alfa Aesar), 1,4-diiodobenzene (98%,

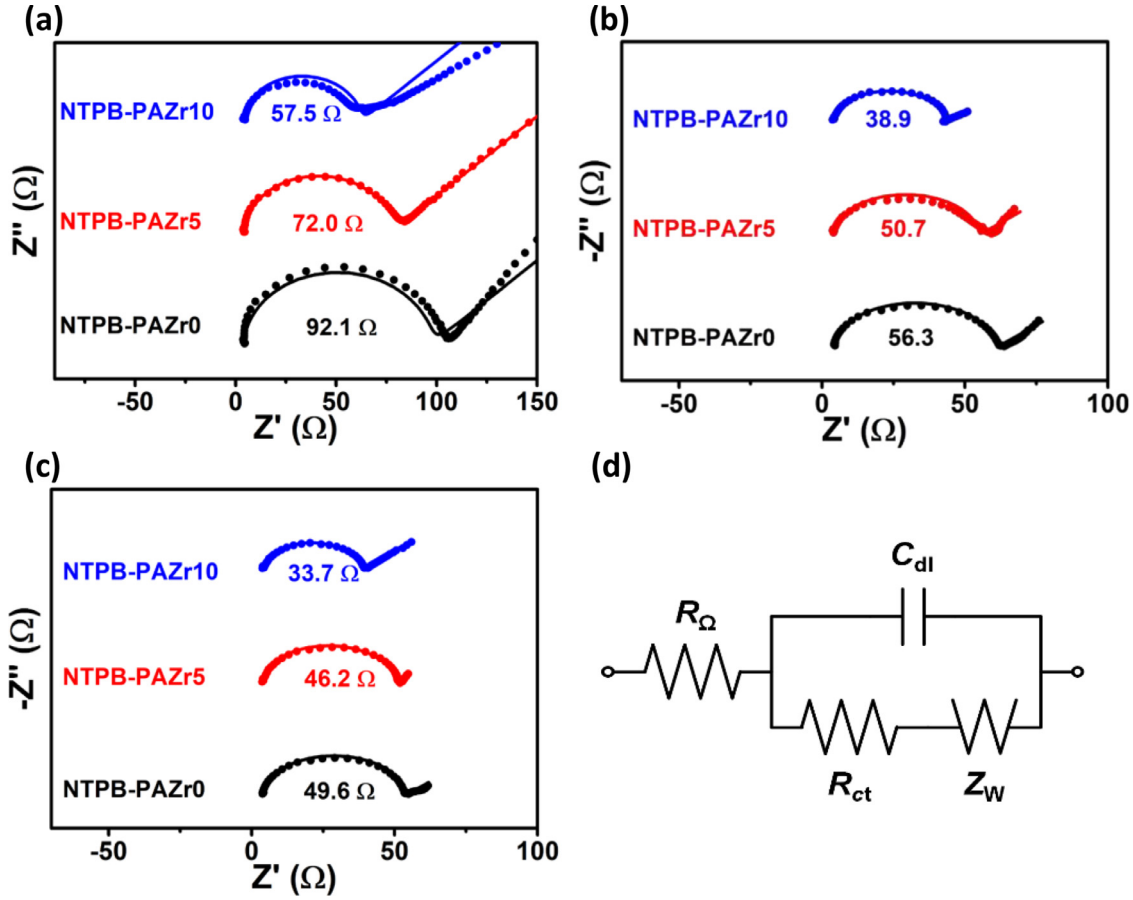

Fig. 7. Nyquist plots of EC films at (a) 0 V, (b) 0.48 V, (c) 0.9 V and (d) Randles circuit.

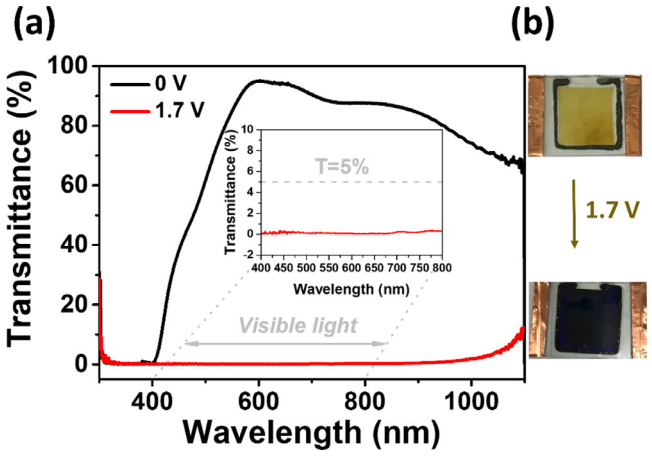

Fig. 9. Transmittance spectra of the gel-type NTPB-PA/HV ECD (deposited area: 20 mm × 20 mm) in 0.1 M (5 μmole) $TBABF_4$/PC at different applied voltages. (b) photos of ECDs at neutral state and coloring state.

Alfa Aesar), tris(dibenzylideneacetone)dipalladium (0) ($Pd_2(dba)_3$) (97%, ACROS), tri-*tert*-butylphosphine ($P(tBu)_3$) (99%, STREM CHEMICAL), sodium *tert*-butoxide (NaO*t*Bu) (98%, ACROS), anhydrous toluene (99.8%, SIGMA-ALDRICH), palladium 10% on activated carbon, hydrazine monohydrate (98+%, Alfa), anhydrous tetrahydrofuran (99%, Acros), malic acid (ACROS), calcium chloride (ACROS), zirconium(IV) butoxide ($Zr(OBu)_4$) solution (TCI), *N,N*-dimethylacetamide (DMAc) (TEDIA), *N*-methyl-2-pyrrolidone (NMP), pyridine (ACROS), triphenyl phosphite (TPP) (ACROS) were used as received without further purification. *N,N*-Dimethyl-*N'*-(4-nitro-phenyl)-*p*-phenylenediamine [13], heptyl viologen tetrafluoroborate [27–30], and tetrabutylammonium tetrafluoroborate ($TBABF_4$) [40] were prepared according to the previous reports.

Fabrication of ECDs: The preparation of the gel-type ECDs is illustrated in Fig. S15 to Fig. S16. First, ITO-coated glass substrates (5 Ω/square) were cleaned by ultrasonication in the sequence of hexane, acetone, and isopropanol, respectively. After that, the EC polyamide **NTPB-PA** was drop-coated onto ITO-coated glass substrates (25 mm × 30 mm). Then, the gap between two pieces of ITO-coated glass substrates was confined to 120 μm by using full-auto dispenser to coat thermoset adhesive with a 20 × 20 mm^2 active area, and cured at 120 °C for six hours and retained a tiny hole for injecting gel electrolyte mixture into the device by means of vacuum encapsulating method. Next, gel mixture based on the copolymer (poly(MMA-HEMA)) of methyl methacrylate (MMA) and (hydroxyethyl)methacrylate (HEMA) was plasticized with propylene carbonate (PC). Then, the gel electrolytes were prepared with 7.6 mg of poly(MMA-HEMA), 1.65 mg (0.1 M) of $TBABF_4$, 0.40 mg (0.015 M) of HV, 0.63 mg of aliphatic polyisocyanate (Desmodur® N3200), 0.01 mg of catalyst dibutyltin diacetate, and 0.05 mL of PC. After injection of gel electrolytes, the tiny hole was sealed by UV-curing adhesive and the device would be cured under 75 °C for two hours.

Supporting Information: Experiment details including monomer and polymer synthesis, measurements, and monomer and polymer characterization. Basic electrochromic properties of ECMs including HV and NTPB-PA. Besides, the electrochromic properties of ECDs derived from NTPB-PA in ambipolar system were also investigated.

Declaration of Competing Interest

The authors declare no competing financial interest.

Authorship contribution statement

G.S.L and F.W.L conceived the study project. G.S.L guided and supervised the project. F.W.L fabricated the devices and performed the measurements. F.W.L, and T.C.Y wrote the first draft of the manuscript. G.S.L revised the manuscript.

Acknowledgment

Guey-Sheng Liou received the financial support from “Advanced Research Center for Green Materials Science and Technology” from The Featured Area Research Center Program within the framework of the Higher Education Sprout Project by the Ministry of Education in Taiwan (109L9006) and the Ministry of Science and Technology in Taiwan (MOST 109-2634-F-002-042). Fang-Wei Li, Tzu-Chieh Yen and Guey-Sheng Liou received the financial support from the Ministry of Science and Technology in Taiwan (MOST 107-2113-M-002-024-MY3 and 107-2221-E-002-066-MY3).

Supplementary materials

Supplementary material associated with this article can be found, in the online version, at doi:10.1016/j.electacta.2020.137474.

References

[1] J.R. Platt, Electrochromism, a possible change of color producible in dyes by an electric field, J. Chem. Phys. 34 (3) (1961) 862–863.
[2] S.K. Deb, A novel electrophotographic system, Appl. Opt. 8 (101) (1969) 192–195.
[3] R.J. Mortimer, A.L. Dyer, J.R. Reynolds, Electrochromic organic and polymeric materials for display applications, Displays 27 (1) (2006) 2–18.
[4] X. An, C.Y. Jimmy, Y. Wang, Y. Hu, X. Yu, G. Zhang, WO_3 nanorods/graphene nanocomposites for high-efficiency visible-light-driven photocatalysis and NO_2 gas sensing, J. Mater. Chem. 22 (17) (2012) 8525–8531.
[5] H. Wei, J. Zhu, S. Wu, S. Wei, Z. Guo, Electrochromic polyaniline/graphite oxide nanocomposites with endured electrochemical energy storage, Polymer (Guildf) 54 (7) (2013) 1820–1831.
[6] H. Li, L. McRae, C.J. Firby, A.Y. Elezzabi, Rechargeable aqueous electrochromic batteries utilizing Ti-substituted tungsten molybdenum oxide based Zn^{2+} ion intercalation cathodes, Adv. Mater. 31 (15) (2019) 1807065.
[7] S.K. Deb, Optical and photoelectric properties and colour centres in thin films of tungsten oxide, Philos. Mag. 27 (4) (1973) 801–822.
[8] M. Weil, W.D. Schubert, International Tungsten industry association: London, UK, 2013, 1–9.
[9] C. Santato, M. Odziemkowski, M. Ulmann, J. Augustynski, Crystallographically oriented mesoporous WO_3 films: synthesis, characterization, and applications, J. Am. Chem. Soc. 123 (43) (2001) 10639–10649.
[10] R.J. Mortimer, Electrochromic materials, Chem. Soc. Rev. 26 (3) (1997) 147–156.
[11] V.D. Neff, Electrochemical oxidation and reduction of thin films of Prussian blue, J. Electrochem. Soc. 125 (6) (1978) 886.
[12] G. Barbarella, M. Melucci, G. Sotgiu, The versatile thiophene: an overview of recent research on thiophene-based materials, Adv. Mater. 17 (13) (2005) 1581–1593.
[13] K. Gurunathan, A.V. Murugan, R. Marimuthu, U.P. Mulik, D.P. Amalnerkar, Electrochemically synthesised conducting polymeric materials for applications towards technology in electronics, optoelectronics and energy storage devices, Mater. Chem. Phys. 61 (3) (1999) 173–191.
[14] C.L. Bird, A.T. Kuhn, Electrochemistry of the viologens, Chem. Soc. Rev. 10 (1) (1981) 49–82.
[15] L. Michaelis, E.S. Hill, The viologen indicators, J. Gem. Physiol. 16 (6) (1933) 859–873.
[16] J.W. Xu, M.H. Chua, K.W. Shah, Electrochromic Smart Materials: Fabrication and Applications, Royal Society of Chemistry, 2019.
[17] H.J. Yen, G.S. Liou, Design and preparation of triphenylamine-based polymeric materials towards emergent optoelectronic applications, Prog. Polym. Sci. 89 (2019) 250–287.
[18] K.Y. Chiu, T.X. Su, J.H. Li, T.H. Lin, G.S. Liou, S.H. Cheng, Novel trends of electrochemical oxidation of amino-substituted triphenylamine derivatives, J. Electroanal. Chem. 575 (1) (2005) 95–101.
[19] H.J. Yen, G.S. Liou, Solution-processable novel near-infrared electrochromic aromatic polyamides based on electroactive tetraphenyl-p-phenylenediamine moieties, Chem. Mater. 21 (17) (2009) 4062–4070.
[20] J.T. Wu, H. t. Lin, G.S. Liou, Synthesis and characterization of novel triarylamine derivatives with dimethylamino substituents for application in optoelectronic devices, ACS Appl. Mater. Interfaces 11 (16) (2019) 14902–14908.
[21] S.H. Hsiao, G.S. Liou, Y.C. Kung, H.J. Yen, High contrast ratio and rapid switching electrochromic polymeric films based on 4-(dimethylamino) triphenylamine-functionalized aromatic polyamides, Macromolecules 41 (8) (2008) 2800–2808.

[22] B.C. Pan, W.H. Chen, T.M. Lee, G.S. Liou, Synthesis and characterization of novel electrochromic devices derived from redox-active polyamide–TiO_2 hybrids, J. Mater. Chem. C 6 (45) (2018) 12422–12428.
[23] G.S. Liou, P.H. Lin, H.J. Yen, Y.Y. Yu, W.C. Chen, Flexible nanocrystalline-titania/polyimide hybrids with high refractive index and excellent thermal dimensional stability, J. Polym. Sci. Pol. Chem. 48 (6) (2010) 1433–1440.
[24] G.S. Liou, P.H. Lin, H.J. Yen, Y.Y. Yu, T.W. Tsai, W.C. Chen, Highly flexible and optical transparent 6F-PI/TiO_2 optical hybrid films with tunable refractive index and excellent thermal stability, J. Mater. Chem. 20 (3) (2010) 531–536.
[25] J.T. Wu, G.S. Liou, A novel panchromatic shutter based on an ambipolar electrochromic system without supporting electrolyte, Chem. Commun. 54 (21) (2018) 2619–2622.
[26] H.S. Liu, B.C. Pan, D.C. Huang, Y.R. Kung, C.M. Leu, G.S. Liou, Highly transparent to truly black electrochromic devies based on an ambipolar system of polyamides and viologen, NPG Asia Mater. 9 (2017) e388.
[27] C.W. Hu, K.M. Lee, K.C. Chen, L.C. Chang, K.Y. Shen, S.C. Lai, T.H. Kuo, C.Y. Hsu, L.M. Huang, R. Vittal, K.C. Ho, High contrast all-solid-state electrochromic device with 2, 2, 6, 6-tetramethyl-1-piperidinyloxy (TEMPO), heptyl viologen, and succinonitrile, Sol. Energy Mater. Sol. Cells 99 (2012) 135–140.
[28] J.H. Wu, G.S. Liou, High-performance electrofluorochromic devices based on electrochromism and photoluminescence-active novel poly (4-cyanotriphenylamine), Adv. Funct. Mater. 24 (41) (2014) 6422–6429.
[29] C.W. Chang, G.S. Liou, Novel anodic electrochromic aromatic polyamides with multi-stage oxidative coloring based on N, N, N′, N′-tetraphenyl-p-phenylenediamine derivatives, J. Mater. Chem. 18 (46) (2008) 5638–5646.
[30] Y. Xiao, L. Chu, Y. Sanakis, P. Liu, Revisiting the IspH catalytic system in the deoxyxylulose phosphate pathway: achieving high activity, J. Am. Chem. Soc. 131 (29) (2009) 9931–9933.
[31] C.H. Chen, F. Fei, N.W. Sun, X.G. Zhao, S.Y. Meng, D.M. Wang, (Jilin University) Diamine monomer containing 4-dimethylamine-substituted tetraphenyl-p-phenylenediamine structure and preparation method and application of diamine monomer containing 4-dimethylamine-substituted tetraphenyl-p-phenylenediamine structure. CN105924361, 2016.
[32] N. Yamazaki, F. Higashi, J. Kawabata, Studies on reactions of the N-phosphonium salts of pyridines. XI. Preparation of polypeptides and polyamides by means of triaryl phosphites in pyridine, J. Polym. Sci. Polym. Chem. Ed. 12 (9) (1974) 2149–2154.
[33] N. Yamazaki, M. Matsumoto, F. Higashi, Studies on reactions of the N-phosphonium salts of pyridines. XIV. Wholly aromatic polyamides by the direct polycondensation reaction by using phosphites in the presence of metal salts, J. Polym. Sci. Polym. Chem. Ed. 13 (6) (1975) 1373–1380.
[34] C.W. Chang, C.H. Chung, G.S. Liou, Novel anodic polyelectrochromic aromatic polyamides containing pendent dimethyltriphenylamine moieties, Macromolecules 41 (22) (2008) 8441–8451.
[35] C.W. Chang, G.S. Liou, S.H. Hsiao, Highly stable anodic green electrochromic aromatic polyamides: synthesis and electrochromic properties, J. Mater. Chem. 17 (10) (2007) 1007–1015.
[36] G.S. Liou, C.W. Chang, Highly stable anodic electrochromic aromatic polyamides containing N, N, N ‘, N ‘-tetraphenyl-p-phenylenediamine moieties: synthesis, electrochemical, and electrochromic properties, Macromolecules 41 (5) (2008) 1667–1674.
[37] R.S. Nicholson, I. Shain, Theory of stationary electrode polarography. Single scan and cyclic methods applied to reversible, irreversible, and kinetic systems, Anal. Chem. 36 (4) (1964) 706–723.
[38] H.J. Yen, S.M. Guo, G.S. Liou, J.C. Chung, Y.C. Liu, Y.F. Lu, Y.Z. Zeng, Mixed–valence class I transition and electrochemistry of bis (triphenylamine)-based aramids containing isolated ether-linkage, J. Polym. Sci. Part A Polym. Chem. 49 (17) (2011) 3805–3816.
[39] C. Lambert, G. Nöll, The class II/III transition in triarylamine redox systems, J. Am. Chem. Soc. 121 (37) (1999) 8434–8442.
[40] J.T. Wu, T.L. Hsiang, G.S. Liou, Synthesis and optical properties of redox-active triphenylamine-based derivatives with methoxy protecting groups, J. Mater. Chem. C 6 (48) (2018) 13345–13351.